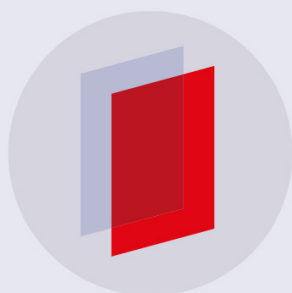# Pulsars with bow shocks: model constraints of the pulsar wind Lorentz factor

To cite this article: A E Petrov *et al* 2018 *J. Phys.: Conf. Ser.* **1038** 012001

View the article online for updates and enhancements.

Related content

IOP ebooks™

Bringing you innovative digital publishing with leading voices to create your essential collection of books in STEM research.

Start exploring the collection - download the first chapter of every title for free.

Pulsars with bow shocks: model constraints of the pulsar wind Lorentz factor

A E Petrov[1], **A M Bykov**[1,2], **S M Osipov**[1], **A M Krassilchtchikov**[1] and **K P Levenfish**[1]

[1]Ioffe Institute, 26 Politekhnicheskaya st., St. Petersburg 194021, Russia
[2]Peter the Great St. Petersburg Polytechnic University, 29 Politekhnicheskaya st., St. Petersburg 195251, Russia

E-mail: `a.e.petrov@mail.ioffe.ru`

Abstract. Pulsar wind nebulae with bow shocks (BSPWNe) can efficiently accelerate electrons and positrons of the pulsar wind (PW). The particles injected into such nebulae at the PW termination shock can gain energy due to the Fermi acceleration in the colliding shock flow between the two shocks. Monte-Carlo modeling of the PW particle transport through the nebula reveals a significant deformation of their spectrum between the shocks in comparison with the injected spectrum. The maximal energies achieved by the hard component of the spectrum ($f(E) \propto E^{-p}$ with $p < 2$) depend on the flow velocities. Comparison of the obtained spectra of the accelerated PW particles in BSPWNe and their synchrotron emission maps with the observational data obtained in the optical, far-UV and X-ray bands allows one to constrain global parameters of particular BSPWNe such as Lorentz-factors of their PWs.

1. Introduction

Multiwavelength observations of pulsar wind nebulae (PWNe) have revealed a vast variety of their morphologies, which can strongly depend on the considered energy range. Spatially resolved emission spectra provide an evidence of evolution of the particle energy distributions in the nebulae.

An example of such evolution is the nebula around PSR J0437-4715 (hereafter J0437). The bow shock (BS) of the pulsar moving at a supersonic velocity $u_{\rm psr} \approx 104$ km s^{-1} through the interstellar medium (ISM) was first detected in H_α [1] and later also seen in the far ultraviolet (FUV) range ($1250 - 2000$ Å, $6.2 - 9.9$ eV) [2]. The observed FUV bow shock luminosity is $L_{\rm FUV} \sim 5 \times 10^{28}$ erg s^{-1} – an order of magnitude higher than the H_α one. However, in the 0.5-7 keV X-rays the BS is absent, and only a faint PWN with luminosity $L_X \sim 3 \times 10^{28}$ erg s^{-1} is observed [2].

The energy dependence of the J0437 morphology could be understood within a model of the synchrotron emission of the relativistic PW particles accelerated in the colliding shock flows (CSFs) between the termination shock (TS) of the PW and the BS. In [3] a Monte-Carlo model of propagation of PW particles through the BSPWN was discussed. The simulation shows that a hard component of particle spectra with $f(E) \propto E^{-p}$, $p < 2$ is formed between the two shocks.

The efficiency of Fermi acceleration in the CSFs depends on the flow velocities. As discussed in [3], trans-relativistic flows are the most efficient sites for the diffusive shock acceleration. Proper velocities of the pulsars $u_{\rm psr}$ usually do not exceed $(1\text{-}2) \times 10^3$ km s^{-1} [4], so the relativistic

velocity of the shocked PW u_{pw} should be the key parameter of the acceleration process [3]. A simple estimation given in [3] shows that in the absence of severe radiative energy losses, the maximal energy gained by the particles accelerated in CSFs scales $\propto \sqrt{u_{pw}}$.

Simulation of BSPWN emission for a range of probable PW velocities allows one to impose constraints on u_{pw}, which is important for studies of non-trivial energy conversion processes in the PW. Here we apply the model developed in [3] to reproduce the observed PWN morphology at various energies and constrain the PW velocity in the J0437 BSPWN.

2. Model Overview
Here we present a brief overview of the Monte-Carlo (MC) model of particle transport in a BSPWN discussed in details in [3].

The MC model takes into account the main geometrical features of a BSPWN and allows us to consider particle escape from the acceleration site, that is essential for modeling of particle acceleration in astrophysical environments. Concentration on the high energy particles emitting synchrotron radiation in the FUV and X-ray bands allows a significant model simplification. Transport of those particles with large mean free paths (mfps) is almost not affected by the complicated structure of flows near the contact discontinuity (CD) between the CSFs. Along with dissipation of magnetic inhomogeneities by CD and deceleration of the flows this grounds the spatial structure of the simulation region (see the sketch in Fig. 1).
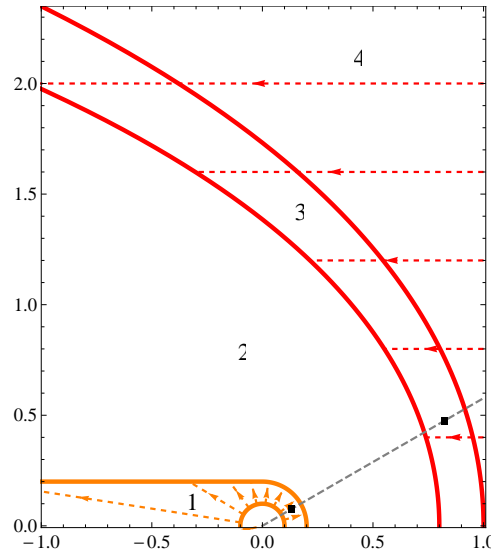

Figure 1. The model geometry: half of the axial section. Region 1 (between the orange curves) – the shocked PW, 2 — region near the contact discontinuity, 3 (between the red curves) — the postshock flow of the ISM matter, 4 — the unperturbed ISM. Black squares mark locations chosen for demonstration of particle distribution function in Fig. 2. The angle between the gray dashed line and the symmetry axis is $30°$.

Particles are injected at the termination shock (TS) of the PW (sphere of radius r_{ts}) and propagate through the axisymmetric system of regions with fixed values of mean magnetic induction, distribution of flow velocities and diffusion parameters. The system has an axial symmetry with axis that coincides the pulsar proper motion velocity vector and is bounded by a cylindrical free escape boundary (FEB) surface. Particle propagation is treated in the pulsar rest frame with consideration that particle scatterings are isotropic in the local plasma rest frame. In Region 2 near the CD the particle advection is neglected. It is separated by a surface given

by (2) from Region 1 – the PWN, where the radially directed flow velocity is given by (1), u_0 is a free parameter of the model (here r is the distance from the pulsar, θ is the angle between its proper velocity and a considered direction; a_{in} – a model parameter).

$$u_{pw} = u_0 \left(\frac{r_{ts}}{r} \right)^2 \tag{1}$$

$$r\left(\theta\right) = \begin{cases} a_{in}, \text{ if } \theta \leq \pi/2 \\ a_{in}/\sin\theta, \text{ if } \theta > \pi/2. \end{cases} \tag{2}$$

$$r\left(\theta\right) = R \csc\theta \sqrt{3\left(1 - \theta \cot\theta\right)}. \tag{3}$$

The borders of Region 3 (the area near the bow shock) are described by equation (3), giving the shape of a BS in the thin shell approximation [5]. The apexes of the inner and outer border positions are free parameters of the model. The flow velocity is uniform in both Regions 3 and 4 (the unperturbed ISM) and equal to u_{psr}.

The growth of cosmic ray (CR) driven instabilities caused by the proton acceleration at the BS can yield a significant growth of magnetic field fluctuations near the BS. It can occur at the wavelengths up to the scale $L_{cor} \gg R_{max}$, where R_{max} is the gyroradius of protons of maximum achieved energy [6]. Hence, the mfps of PW particles propagating through the BS region are likely defined by a Bohm-like diffusion coefficient up to the Lorentz-factor γ_1 defined as $r_g\left(\gamma_1\right) = L_{cor}$, where $r_g\left(\gamma\right)$ is the gyroradius of a particle with the Lorentz-factor γ in the local mean magnetic field. In the model γ_1 is considered as a free parameter, and the mfps in Regions 2 and 3 are $\sim r_g$ for $\gamma < \gamma_1$ and correspond to a short-scale scattering mode $\propto \gamma^2$ otherwise (see [3] for more details). In the PWN we use mfp $\propto r_g$, while in the ISM an estimation obtained from the galactic CR propagation models is employed (see, e.g. [7]).

The Monte-Carlo modeling allows one to obtain the particle distribution function at the grid of bins in the phase space (see [3]). The PWNe emission is affected by the Doppler boosting, which is taken into account. The particle acceleration is related to anisotropy of particle distribution (e.g., currents), which may be strong enough in the case of relativistic flows. Binning of all particle momentum components allows one to obtain the distribution function averaged over an arbitrary small solid angle element along a given direction. That makes possible calculation of particle emission with an account of an anisotropy of their distribution. In practice, the accuracy of the obtained particle angular distribution is limited by available computational resources.

Due to the axial symmetry of the source its appearance for the observer depends on its orientation. The angle Θ between the pulsar proper motion velocity and the direction from the observer to the pulsar is a free parameter of the model. We use $\Theta = 90°$.

3. Simulated particle and emission spectra

In the left panel of Figure 2 the simulated particle spectra are shown. The particle energy distributions at the locations indicated by black squares in Figure 1 are presented. Distribution functions $f\left(E\right)$ are normalized so that the mean concentration $n = \int f\left(E\right)dE$ ($E = mc^2\gamma$ is the particle energy, m – the electron mass) and multiplied by E^2. Red color corresponds to the PW velocity at the TS $u_0 = 0.2\,c$, green — to $0.4\,c$, blue — to $0.6\,c$. The black curve shows the spectrum close to the one injected at the TS. The latter was set as a power law $f\left(E\right) \propto E^{-2.3}$ for $\gamma_{min} = 4 \times 10^5 \leq \gamma \leq \gamma_{max} = 2 \times 10^8$.

As expected, a hard component $f\left(E\right) \propto E^{-p}$ with $p < 2$ is formed in some range of energies $E_{\min}\left(u_0\right) < E < E_{\max}\left(u_0\right)$ in both discussed regions (in the case of Region 3 the spectra at low energies are also modified by the flow modulation). One can see that $E_{\max}$ grows with increasing u_0.
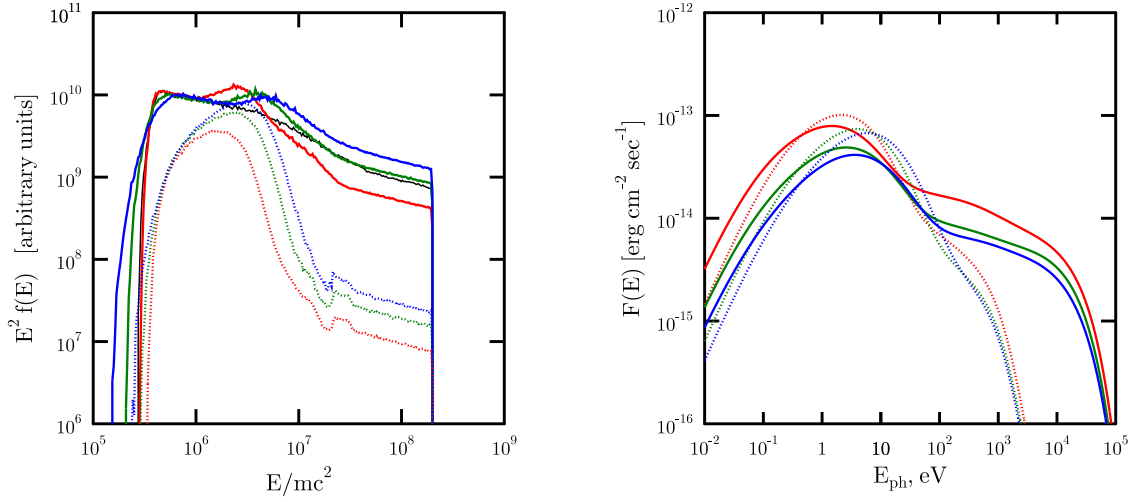
Figure 2. Left: Particle energy distribution in the head parts of the PWN (solid lines) and at the bow shock (dotted lines). Right: Synchrotron spectra of the PWN (solid lines) and of the bow shock region (dotted lines). The red curves correspond to $u_0 = 0.2\,c$, green – to $0.4\,c$ and blue – to $0.6\,c$. The black curve in the left image shows the spectrum close to the one injected at the TS.

In the right panel of Figure 2 the modelled spectra of synchrotron emission (in units $\sim$ erg cm^{-2} sec^{-1}) from the PWN (solid lines) and from the BS region (dotted lines) are shown. The colors correspond to the same values of u_0 as in the left panel, and the fluxes for each setup are normalized in such a way that the observed FUV flux from the 32 arcsec^2 region at the bow shock of J0437 used in [2] is reproduced. Like in the case of particle energy distributions, the range of relatively hard spectrum achieves larger photon energies with the growth of u_0. It also should be emphasized, that in agreement with the observed structure of J0437, at soft X-ray energies (about a few keV) the simulated flux from the BS is much smaller than one from the PWN. In the following section we demonstrate it one more time with simulated images of J0437.

4. Synchrotron images

In Figure 3 the simulated synchrotron images of the object similar to J0437 are shown. Images show the intensity maps of the source, integrated over the spectral range – $(6.2 - 9.9)$ eV in the FUV and $(0.5 - 7)$ keV in the X-rays. The intensity is given in units of (photons cm^{-2} sec^{-1} sr^{-1}) and is normalized in the same way as the integrated fluxes discussed above.

One can see that in all cases the observed morphological features of J0437 are well represented: the bow shock is seen in the FUV images and is absent in the X-ray images. The increasing efficiency of particle acceleration with the growth of u_0 leads to a relative dimming of the PWN images.

To quantitatively compare the model with the observational data we have calculated the luminosities of the PWN in the X-ray band and of the bow shock region in the FUV band and in the 32Å band around the Hα line $(6550 - 6582$ Å$)$. The ratios of the luminosities are summarized in Table 1.

In the case of $u_0 = 0.2\,c$ the ratio $L_{\text{FUV}}/L_{\text{X}}$ is significantly smaller than the observed value that is about 1.7. This is likely due to a modest particle acceleration in the case of a relatively small pulsar wind velocity. However, in all cases the simulated ratios $L_{\text{FUV}}/L_{\text{H}\alpha}$ are
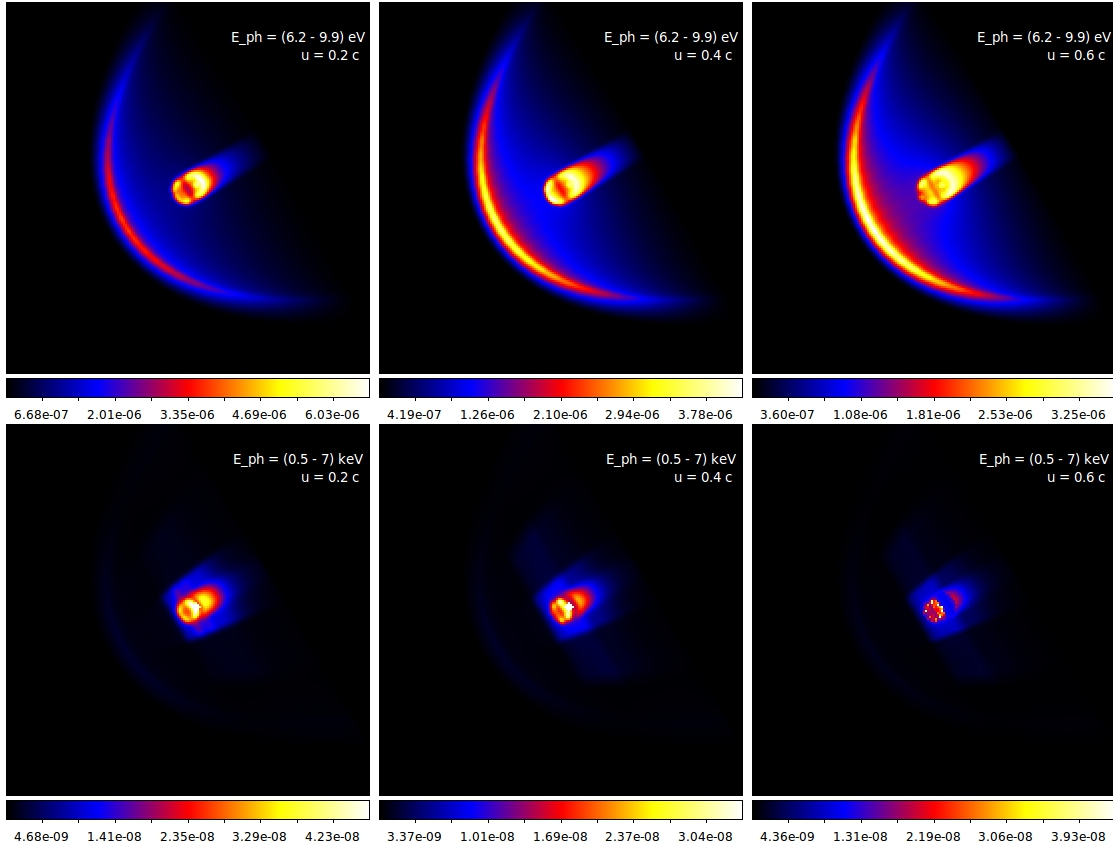
Figure 3. Simulated synchrotron images of a source similar to J0437-4715 in the FUV $(6.2 - 9.9$ eV; top row) and X-ray $(0.5 - 7$ keV, bottom row) bands. Left column: $u_0 = 0.2\,c$, middle — $0.4\,c$, right — $0.6\,c$. The intensities for each value of u_0 are normalized in such a way that the flux from the bow shock reproduces the observed one.

Table 1. The ratios of the modelled PWN and BS luminosities.

	$u_0 = 0.2\,c$	$u_0 = 0.4\,c$	$u_0 = 0.6\,c$
$L_{\mathrm{FUV}}/L_{\mathrm{X}}$	1.2	1.9	2.2
$L_{\mathrm{FUV}}/L_{\mathrm{H}\alpha}$	82	126	158

overestimated compared to the observed $L_{\mathrm{FUV}}/L_{\mathrm{H}\alpha} \sim 10$. This does not mean that the model contradicts the observations as the main contribution to the observed Hα emission is likely provided by the ISM gas heated at the bow shock, which we do not consider.

5. Conclusions
The ability of the Monte-Carlo model of relativictic PW particle transport through a BSPWN developed in [3] to constrain global parameters of pulsar wind has been demonstrated. The model allows one to simulate propagation of a particle population injected into a PWN at the TS through the zone of colliding flows between the TS and the bow shock where particles can be efficiently accelerated. The acceleration causes reshaping of particle energy distribution – a spectral component harder than injected spectrum is formed. The maximal energy achieved by

this component depends on the PW velocity. The model allows to obtain the particle momentum distribution and calculate the spatial distribution of synchrotron emission radiated by the accelerated particles with an account for Doppler boosting and anisotropy of the distribution. In particular, an object similar to the BSPWN of J0437 has been simulated. The model synchrotron images in the FUV $(6.2 - 9.9\,\text{eV})$ and X-ray $(0.5 - 7\,\text{keV})$ ranges reproduce the observed properties of the J0437 morphology for a whole range of PW velocities: the bow shock observed in the FUV is almost absent in the X-rays. However, the simulated ratios of the bow shock FUV luminosty to the PWN X-ray luminosity show, that PW velocities $u_0 \leq 0.2\,c$ appear too low to provide sufficiently strong particle acceleration and thus can be excluded for the modelled source.

Acknowledgments

References

[1] Brownsberger S and Romani R W 2014 *ApJ* **784** 154 (*Preprint* `1402.5465`)
[2] Rangelov B, Pavlov G G, Kargaltsev O, Durant M, Bykov A M and Krassilchtchikov A 2016 *ApJ* **831** 129 (*Preprint* `1605.07616`)
[3] Bykov A M, Amato E, Petrov A E, Krassilchtchikov A M and Levenfish K P 2017 *Space Sci. Rev.* **207** 235–290 (*Preprint* `1705.00950`)
[4] Hobbs G, Lorimer D R, Lyne A G and Kramer M 2005 *MNRAS* **360** 974–992 (*Preprint* `astro-ph/0504584`)
[5] Wilkin F P 1996 *ApJ* **459** L31
[6] Bykov A M, Brandenburg A, Malkov M A and Osipov S M 2013 *Space Sci. Rev.* **178** 201–232 (*Preprint* `1304.7081`)
[7] Strong A W, Moskalenko I V and Ptuskin V S 2007 *Annual Review of Nuclear and Particle Science* **57** 285–327 (*Preprint* `arXiv:astro-ph/0701517`)